*Journal of Mining and Metallurgy 44 B (2008) 39 - 48*

Journal of
Mining and
Metallurgy

# GENERALIZED ELLINGHAM DIAGRAMS FOR UTILIZATION IN SOLID OXIDE FUEL CELLS

**H. Kishimoto, K. Yamaji, M. E. Brito, T. Horita and H. Yokokawa**

National Institute of Advanced Industrial Science and Technology (AIST),
Energy Technology Research Institute
Higashi 1-1-1, Tsukuba Ibaraki 305-8565, Japan

*Dedicated to Prof. Ing. Jaroslav Šesták, DrSc. at the occasion of his 70$^{th}$ birthday*

*(Received 01 September 2008; accepted 10 November 2008)*

## Abstract

*Generalized Ellingham diagram for the P-O-H and the Ni-P-OH systems have been constructed to investigate thermodynamically the chemical stability of nickel anode against the gaseous impurities containing phosphorous compounds. In the same way as the original Ellingham diagram, the oxygen potential is used as the vertical axis, while the temperature is adopted as horizontal axis. For the P-O-H system which contains many gaseous species, the dominant areas of gaseous species are displayed with a parameter of their partial pressure in an analogous way to the aqueous species in the Pourbaix diagram. The multicomponent Ellingham diagram for the Ni-P-O-H system was constructed in a similar manner to the multicomponent Pourbaix diagram. The obtained diagrams have been discussed to examine the reactivity of nickel anodes with phosphorus compounds in SOFCs in terms of operational variables such as temperature, oxygen potential, overpotential under the anode polarization and so on.*

*Keywords: solid oxide fuel cells, SOFC, Ni anode, phosphor poisoning, Ni-P-O system, NI-P-O-H system, nickel phosphates, Pourbaix diagram, Ellingham diagram*

## 1. Introduction

In recent years, there are growing interests in applications of the thermodynamic database and related software to practical material issues [1-4]. As software, the complicated chemical equilibrium calculations and the chemical

* *Corresponding author: h-yokokawa@aist.go.jp*

DOI:10.2298/JMMB0801039K

potential diagrams are most important in high temperature materials science. Since the chemical equilibrium calculations provide results easily to be understood, this has been widely utilized particularly for the multicomponent systems. In contrast, the chemical potential diagrams can be regarded as well organized compilation of equilibrium states. Even so, it needs to establish an easy but powerful method of constructing the chemical potential diagram for the multicomponent system and applying those diagrams to practical materials issues. Yokokawa et al. have proposed the generalized computer program based on the polyhedron approach to construct the generalized chemical potential diagrams for the multicomponent system [5,6]. As one of example of its applications, this was applied to the semi-conducting materials [7].

In the present investigation, the generalized chemical potential diagram is applied to the extension of the Ellingham diagram [8] for the multicomponent systems which are related to the solid oxide fuel cells [9,10]; in this applications, temperature and oxygen potential are the most important among many other thermodynamic variables so that the Ellingham diagram becomes appropriate in representing the chemical equilibria associated with stability and durability of SOFC materials. Recent progress in the SOFC technology makes it necessary to establish the durability of SOFC materials [11,12]. For establishment of long life more than 40,000 h, it has been clarified that the impurities such as sulfur, phosphor, sodium, silicon and halogens should be carefully examined on their effects on electrode activities [13]. In this paper, the procedure of constructing the generalized Ellingham diagrams for the multicomponent systems and is described first and then construction will be made on the Ni-P-O-H system which is needed to examine the degradation of the nickel anodes due to the phosphor contamination in fuels [14-16].

## 2. Thermodynamic data

The thermodynamic data used in the present study is from the thermodynamic database MALT for windows [1-4] except for some compounds in the Ni-P-O system. Table 1 summarizes the thermodynamic data evaluated/estimated in the present investigation.

## 3. Construction Procedures

In the present investigation, almost all diagrams were constructed by using the computer program CHD for constructing generalized chemical potential diagrams [5]. Some parts have been modified to adjust to requirements for constructing Pourbaix diagrams or Ellingham diagrams.

### 3.1 Typical Ellingham Diagram for solid oxide fuel cell materials

Figure 1 shows a typical Ellingham diagram, in which equilibria between $H_2O/H_2$, NiO/Ni, and others are presented in a $\mu(O_2)$ vs. $T$ plot. As the vertical axes, three variables are presented in the right hand side. The logarithmic partial pressure of oxygen molecules is a typical measure to examine the cathode material behavior in air or cathodic polarized states. The logarithmic ratio of partial pressure of $H_2O$ to $H_2$ is instead a measure for anode compartment. As typical anode, nickel is used so that the

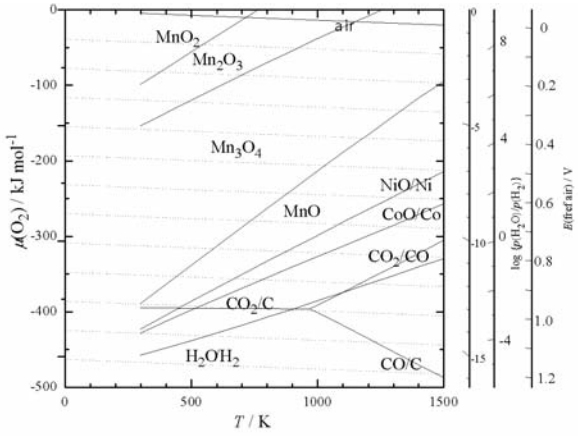


*Figure 1. Ellingham diagram for solid oxide fuel cell related materials (Ni-O. Co-O and Mn-O systems are included in addition to H-O, C-O fuel systems).*

equilibrium between NiO/Ni is critically important. As a third axis, the electrical potential is given which corresponds to the electrical potential of electrodes referred to air. Those scales are in parallel to the line corresponding to the partial pressure of oxygen in air.

For the Mn-O system, borderlines between two adjacent phases are given. In other words, one phase has two borderlines at the upper and lower bounds in the oxygen potential. This is the stability polygon of the phase in the $\mu(O_2)$ vs. $T$ plot. In the generalized chemical potential diagram without specification of temperature values, we have three thermodynamic variables, namely, temperature, oxygen potential and the manganese chemical potential. In Fig. 1, no information on $\mu$(Mn) appears. Thus, the construction of the Ellingham diagram by using the program for constructing generalized chemical potential diagrams can be easily made.

### 3.2 Multicomponent systems

In more complicated systems, similar Ellingham diagrams can be constructed by adopting the following sequence:

1) Select the temperature as one of the changeable thermodynamic variable.

2) Select the oxygen potential as one of possible thermodynamic variables.

3) Construct a two dimensional diagram by fixing some selected chemical potential values.

4) Or construct a three dimensional diagram by fixing an appropriate number of chemical potentials. Then display parts of them in a two dimensional diagram.

### 3.3 Analogous treatments to the generalized Pourbaix diagrams

In practical applications of Pourbaix diagrams to the industrial materials or environments, many useful treatments have been tested with great success. Thus, it will be quite reasonable to adopt similar treatments in the generalized Ellingham diagrams. These can be summarized as follows;

1) Partial pressure of gaseous species. Equilibria among gaseous species or at solid/gas interfaces strongly depend on the partial pressures of gaseous species. This is analogous to the activity (concentration) of aqueous species in the Pourbaix diagram. This can be made by fixing the partial pressures of gaseous species when the chemical potential diagrams are constructed.

2) In a Pourbaix diagram, the redox element is selected and only phase equilibria in which such redox element is involved are presented in a diagram. This can be made in the constructed generalized diagrams by

making the stability polygons (polyhedrons) transparent for those compounds/species which do not contain the redox element. For this purpose, the three dimensional diagram is convenient because other phase equilibria can be explicitly displayed after the above procedure is made. To be consistent with other Ellingham diagrams, three dimensional diagram can be projected on the two dimensional space.

## 4. Ellingham diagrams for the Ni-P-O-H systems

### 4.1 Diagrams for the P-O-H system

Figure 2 shows the three dimensional Ellingham diagram for the P-O-H system. Here the partial pressure of gaseous species belonging to the O-H subsystem is all fixed at 1 atm, while the partial pressure of phosphor containing species is fixed at $10^{-6}$ atm for (a) and (b) and $10^{-9}$ atm for (c). All stable compounds and gaseous species are shown in the $\mu(P)$-$\mu(O_2)$-T space. Comparison between Fig.2(a) and 2(b) clearly indicates how the polygons for $H_2(g)$, $H_2O(g)$, and $O_2(g)$ can be made as transparent in the multicomponent Ellingham diagram. Comparison between Fig. 2(b) and Fig. 2(c) indicates the effect of partial pressure of gaseous species on the predominant area of respective species. With decreasing partial pressure, those molecules having small number of atoms per molecule become more stable and as a result, have a wider predominant area. In the P-O-H system, phosphor oxygen molecules are dominant in the $H_2O$-rich region, while the $PH_3$ and other P-H species become dominant

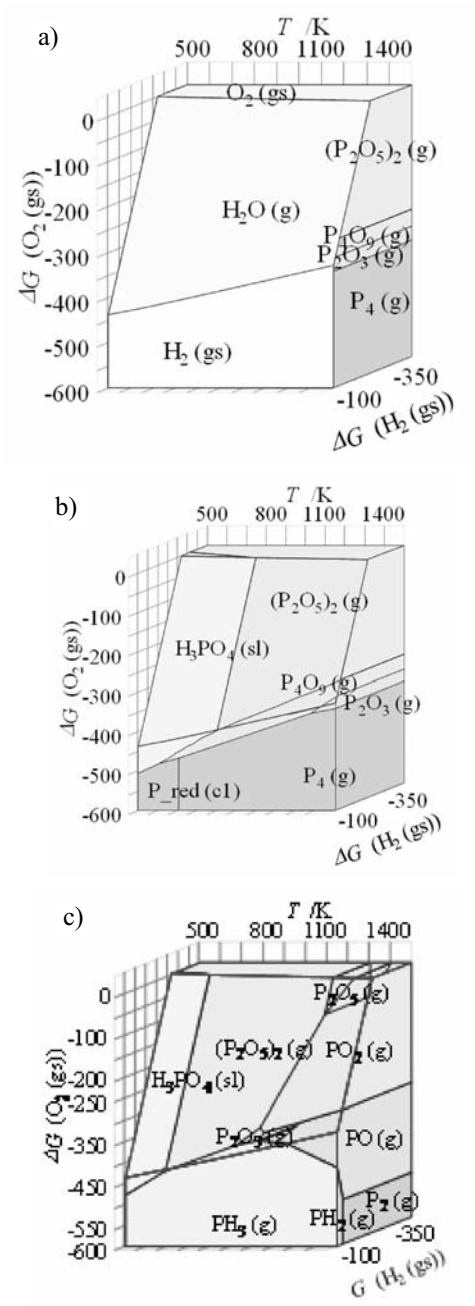


*Fig. 2 Three dimensional Ellingham diagram for the P-O-H system; (a) All stable polygons/polyhedrons for p(PX) = $10^{-6}$ atm are displayed, (b) polygons for $O_2$, $H_2$, $H_2O$ are made transparent; their boundaries are shown on other polyhedrons; (c) stable polyhedrons for p(PX) = $10^{-9}$ atm.*

in the $H_2$-rich region.

In Fig. 3, effect of the partial pressure is more explicitly shown in the two dimensional Ellingham diagram for p(PX)=1, $10^{-3}$, $10^{-6}$, and $10^{-9}$ atm, respectively. Note that the borderline of the $H_2$-dominant and $H_2O$ dominant regions is also given in Fig. 3. This borderline is very important in the solid oxide fuel cells because hydrogen is electrochemically oxidized in the anode compartment so that the atmosphere in anode has the oxygen potential near to this borderline.

### 4.2 Chemical potential diagram for the Ni-P-O system

In the Ni-P-O system, there are several stable intermetallic compounds such as $Ni_3P$ as listed in Table 1. In addition, there are three stable nickel phosphates; namely, $Ni_3(PO_4)_2$, $Ni_2P_2O_7$ and $NiP_2O_6$. The stability of these compounds can be shown in a normal chemical potential diagram like Fig. 4. Since the stabilization energy of nickel phosphates from the constituent oxides is larger compared with the

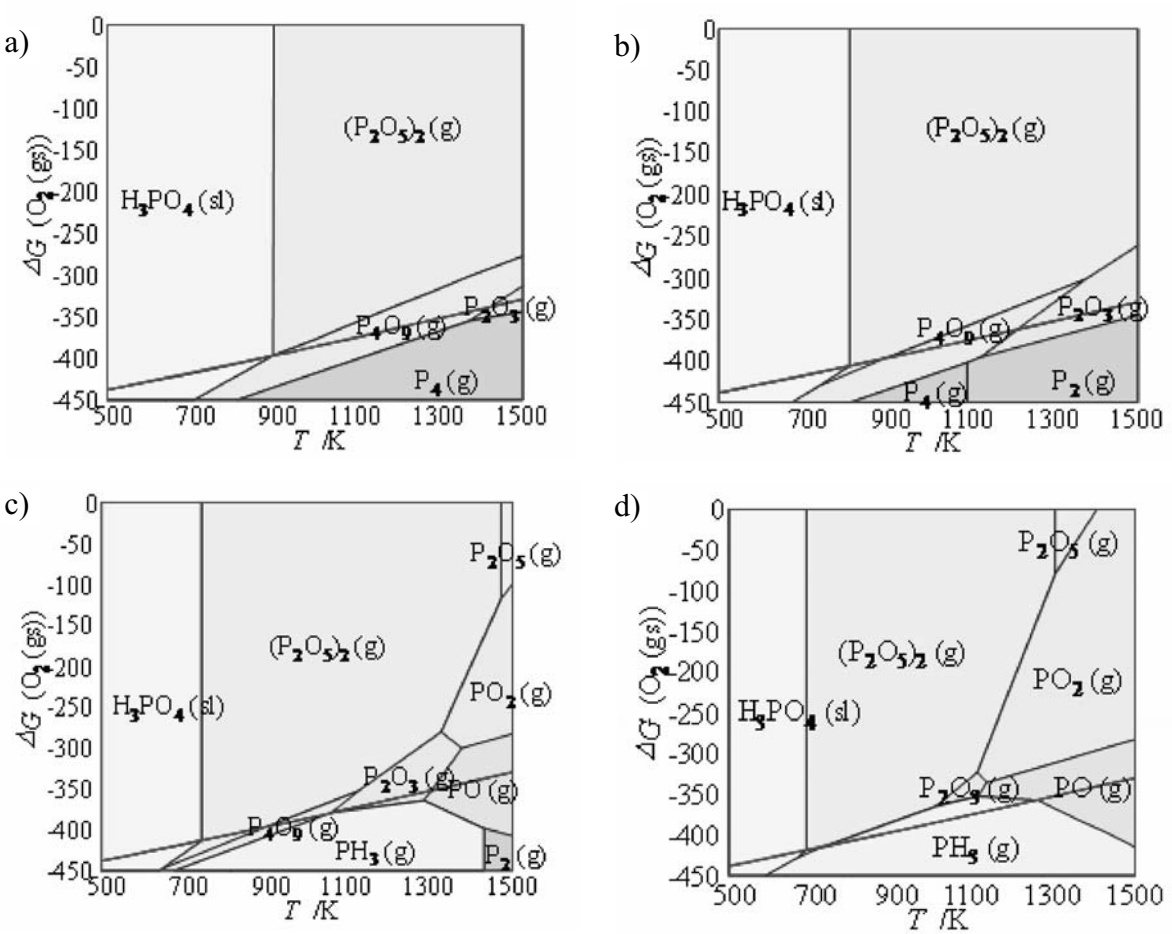


*Fig. 3 Two dimensional Ellingham diagrams for the P-O-H system at the selected partial pressures for the gaseous species; (a) p(PX) = 1 atm; (b) p(PX) = $10^{-3}$ atm; (c) p(PX)=$10^{-6}$ atm; (d) p(PX) = $10^{-9}$ atm.*

*Table 1. Thermodynamic properties of components of ideal association solutions used in the present investigation: ΔfH, the enthalpy change for formation; S, entropy at 298 K, a, b, c, d, e coefficients of heat capacity equation, $C_p$/ J $K^{-1}$ $mol^{-1}$ = a + b *$10^{-3}$T/K + c*105 $(T/K)^{-2}$ + d*$10^{-6}$ $(T/K)^2$ + e*108 $(T/K)^{-3}$; Tlimit, temperature limit of equation.*

| Compound | state | $\Delta_f$H kJ/mol | S J/K mol | a | b | c | d | e | $T_{limit}$ | ref |
|---|---|---|---|---|---|---|---|---|---|---|
| $NiP_2O_6$ | c | -1926.7 | 152.42 | 179.326 | 42.056 | -47.498 | 0 | 0 | 1553 | * |
| $Ni_2P_2O_7$ | c | -2282.25 | 190.41 | 227.216 | 48.836 | -52.808 | 0 | 0 | 1668 | * |
| $N_3(PO_4)_2$ | c | -2580.15 | 228.4 | 275.106 | 55.616 | -58.118 | 0 | 0 | 1623 | * |

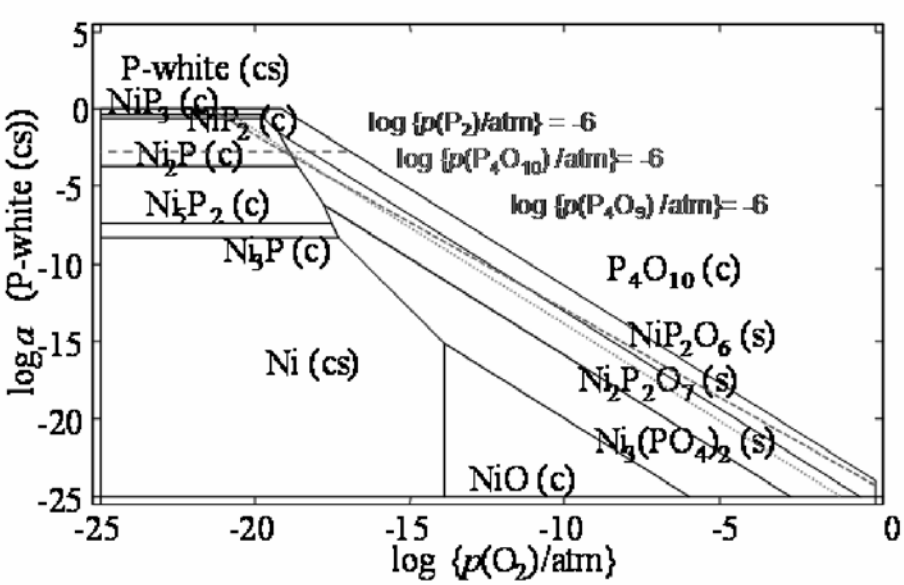


*Fig. 4 Two dimensional chemical potential diagram for the Ni-P-O system in a log {$p(O_2)$/atm} vs. log a(P) plot at 1073 K. The iso partial pressure lines are displayed for $P_2$(g), $P_4O_9$, and $P_4O_{10}$ at $10^{-6}$ atm. Compare with Fig. 3(c) for p(PX)= $10^{-6}$ atm.*

stabilization energy in alloys, the stability areas of nickel phosphates extend to the more reduced atmosphere compared with NiO. In the same diagram, iso partial pressure lines for $P_2$(g), $P_4O_9$(g) and $P_4O_{10}$(g) at p(PX)=$10^{-6}$ atm are displayed, since those species can be dominant species.

### 4.3 Ellingham diagram for the Ni-O-H system

In Fig.5, the Ellingham diagram for the Ni-O-H system is shown. Although this diagram is well established, the predominant areas for nickel gaseous species are also included to compare the behavior with those in the P-O-H system. Here again, the

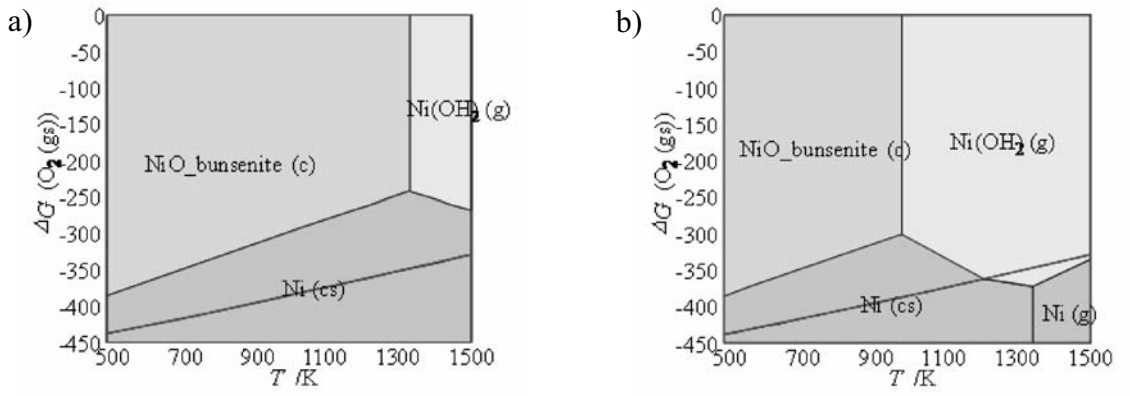


*Fig. 5 Two dimensional Ellingham diagram for the Ni-O-H system under the conditions of (a) p(NiX)=$10^{-6}$ atm and (b) p(NiX)=$10^{-9}$ atm*

borderline for the $H_2$- and the $H_2O$ dominant regions is indicated. Since the nickel anode activity is heavily degraded when nickel is oxidized, the nickel metal stable region is highly important in the solid oxide fuel cells.

### 4.4 Extended Ellingham diagrams for the Ni-P-O-H system

The Ellingham diagrams for the Ni-P-O-H system shown in Fig. 6 were constructed as follows; first, the three dimensional Ellingham diagrams were constructed under the conditions of p($H_2$) = 1 atm or p($H_2O$) = 1 atm. Those diagrams are projected into a normal two dimensional diagrams. Two diagrams can be joined with each other on the borderline between the $H^{2-}$ and $H_2O$-dominant regions. In Fig.6, it will not be difficult this borderline is actually indicated. In Fig. 6, those gaseous species appearing in Figs. 2 and 3 were treated as transparent species. Their predominant are not explicitly shown but only the borderlines are displayed. As a result, Fig. 6 collects the stability areas of those compounds/species which always include nickel. In other words, Fig. 6 is the predominant diagram for nickel

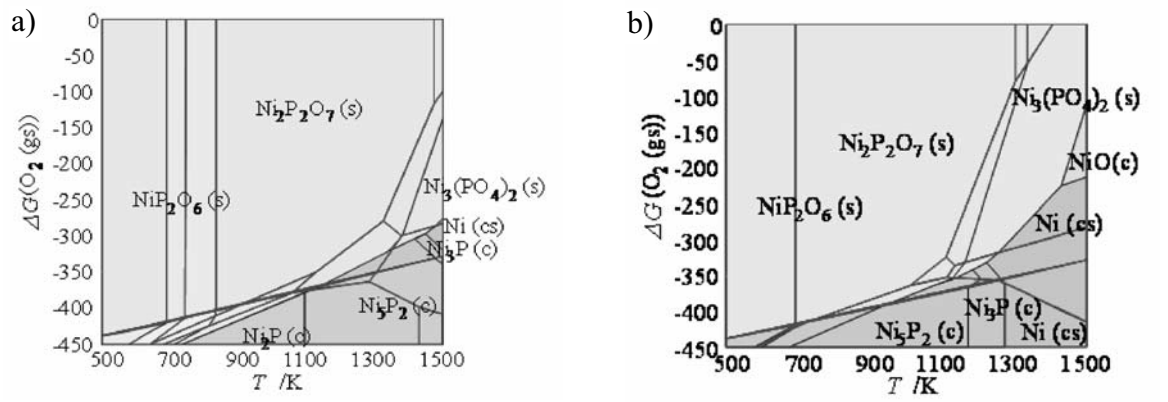


*Fig. 6 Ellingham diagrams for the Ni-P-O-H system under the conditions of (a) p(PX)=$10^{-6}$ atm and (b) p(PX)=$10^{-9}$ atm.*

compounds/species in the plot of Ellingham type. In this sense, the Ellingham diagram for the multicomponent system exhibits similarity to the Pourbaix diagrams for the multicomponent systems.

From the physicochemical point of view, Fig. 6 indicates the interesting behaviors in the Ni-phosphor interactions in the $H_2/H_2O$ environment.

(1) Since the Ni-P interaction is strong, the Ni phosphides are formed even under the condition of $p(PX)=10^{-9}$ atm. Since the dominant phosphor containing species is PH3, this reaction can be written down as follow;

$$2PH_3(g) + 5Ni = Ni_5P_2 + 3H_2(g) \quad [1]$$

(2) In the oxygen potential region where PH3 is oxidized into $P_2O_3(g)$ or $P_4O_9(g)$, nickel can be reacted with phosphor gaseous species to form nickel phosphates;

$$2PH_3(g) + 5O_2(g) + 2Ni = Ni_2P_2O_7 + 3H_2O(g) \quad [2]$$

Or

$$4PH_3(g) + 8O_2(g) = (P_2O_5)_2(g) + 6H_2O(g) \quad [3]$$

$$(P_2O_5)_2(g) + 4Ni + 2O_2(g) = 2Ni_2P_2O_7 \quad [4]$$

Since this phosphate formation reaction can be take place in the original Ni-dominant region shown in Fig. 6, the interaction of Ni with phosphorous oxides is extremely strong.

## 5. Discussions

The electrochemical investigations on effect of phosphor impurities on nickel anode activity have been recently made in relation to the utilization of coal gasified gas. For example, Zhi et al.[16] have recently reported the experimental results of introducing about 20 ppm of $PH_3$ in Syngas for 8-12 h. They observed the following interesting features;

(1) Nickel is reacted with $PH_3$ in the anodic polarization to form $Ni_3(PO_4)_2$, leading rapid degradation of anode performance;

(2) In addition, they observed the formation of $ZrP_2O7$. This Zr is originated from the yttria stabilized zirconia used as the oxide component in the nickel cermet (ceramics and metal) electrodes.

(3) Under the OCV condition, P and Zr coexist in the outer surface of nickel cermet, whereas only the P was detected in the outer region under the potentiostatic operation at 0.7 V.

In order to interpret those phenomena, additional diagrams were constructed and shown in Fig. 7. This is essentially the same as Fig. 4, but explicitly indicates the effects of gaseous species in another type of plot. This indicates that at 1073 K, nickel is in equilibrium with $Ni_3(PO_4)_2$. This confirms that the coexistence of Ni and $Ni_3(PO_4)_2$ is a result of consumption of gaseous phosphor containing species to form $Ni_3(PO_4)_2$ and resulting decrease in the partial pressure of phosphor containing gases. The difference in appearance between the OCV and cathodic polarization can be interpreted in terms of the oxygen potential difference in the two cases; that is, under the OCV condition, the oxygen potential is rather low so that the Ni phosphides are first formed, whereas the nickel phosphates can be directly formed as a reaction among the

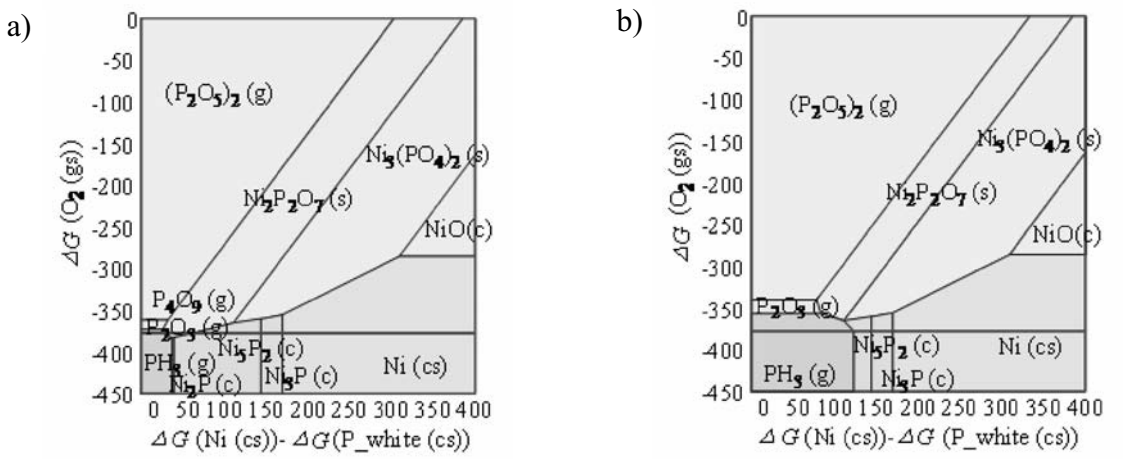


*Fig. 7 Chemical potential diagram for the Ni-P-O-H system at 1073 K. The upper part corresponds to the condition of $p(H_2O)$ = 1 atm, the lower being $p(H_2)$ = 1 atm. (a) the partial pressure of PX is fixed at $10^{-6}$ atm; (b) the partial pressure of PX is fixed at $10^{-9}$ atm.*

nickel anode, emitted water vapor and the phosphor containing species. The latter may cause to hider the $ZrP_2O_7$ formation. In more detailed analysis, the chemical potential diagrams which contain Zr as the main component are highly required.

## 6. Conclusions

The present investigation has revealed that the Ellingham diagram can be easily extended to the muticomponent systems by adopting the available procedures of handling the stability area in the thermodynamic MALT database and associated CHD software to constructing generalized chemical potential diagrams. The application to the Ni-P-O-H system has been successfully made to construct the various type of diagrams which can be easily compared with the experimental features in the electrochemical operations in which temperature and oxygen potential are key variable. In addition, phase equilibria given in terms of oxygen potential is important when consideration is made on the effect of polarization causing overpotential inside the electrode layer. The present diagrams for the Ni-P-O-H system are found to be well consistent with the experimentally reported features of reaction of nickel anode with phosphor containing syngas.

## References

1. H. Yokokawa, S. Yamauchi, T. Matsumoto, "Thermodynamic database MALT2 and its applications to high temperature materials chemistry," *Thermochimica Acta* 245 (1994) 45 .

2. H. Yokokawa, T. Matsumoto, S. Yamauchi, “Applications of Thermodynamic Database MALT2 to Materials Chemistry: Representation of Reaction Path in Generalized Chemical Potential Diagrams,” proc. 9th Intntl. Conf. High Temperature Materials Chemistry,” ed. K. E. Spear, PV97-39, The Electrochem. Soc. 1997, pp. 250-257.

3. H. Yokokawa, S. Yamauchi and T. Matsumoto, "The Thermodynamic Database MALT," *CALPHAD,* 23(2-4)(1999) 357.

4. H. Yokokawa, S. Yamauchi, and T. Matsumoto, "Thermodynamic Database MALT for Windows with gem and CHD," *CALPHAD,* 26(2)(2002) 155.

5. H. Yokokawa, K. Yamaji, T. Horita, N. Sakai, "A Convex Approach of Constructing Chemical Potential Diagrams for Multi Component Systems," *CALPHAD*, 24(4)(2001) 435.

6. H. Yokokawa, "Generalized Chemical Potential Diagram and its Applications to Chemical Reactions at Interfaces between Dissimilar Materials," *J. Phase Equilibria,* 20(3)(1999) 258.

7. J. Sestak, J. Leiner, H. Yokokawa, B. Stepanek, "Thermodynamics and phase equilibria data in the S-Ga-Sb system auxiliary to the growth of doped GaSb single crystals," *Thermochimica Acta,* 245(1994) 189.

8. M. Pourbaix and X-Z. Yang, "Chemical and Electrochemical Equilibrium Diagrams in the Presence of a Gaseous Phase," pp. 59-89, in "Diagrams of Chemical and Electrochemical Equilibria, Their Setting up and Applications," proc. Of a NATO Advanced Research Workshop (22nd CEFA Seminar), Ed. M. Pourbaix and A. Pourbaix, CEBELCOR, 1982.

9. N. Q. Minh and T. Takahashi, "Science and Technology of Ceramic Fuel Cells," Elsevier, Amsterdam, 1995.

10. S. C. Singhal and K. Kendall ed. "High Temperature Solid Oxide Fuel Cells: Fundamentals, Design and Applications," Elsevier, Amsterdam, 2003.

11. H. Yokokawa, H. Tu, B. Iwanschitz, A. Mai, "Fundamental Mechanism Limiting Solid Oxide Fuel Cell Durability," *J. Power Sources,* 182(2008) 400.

12. H. Yokokawa, "Part 5.5 Performance and Degradations, Chapter Overview of Solid Oxide Fuel Cell Degradation," to be published in "Handbook of Fuel Cells Fundamentals Technology and Application, Vols. 5 and 6. Advances in Electrocatalyst, Materials, Diagnotics, and Durability, ed. W. Vielstich, H. A. Gasteiger and H. Yokokawa, John Wiley & Sons, (2009).

13. H. Yokokawa, N. Sakai, T. Horita, and K. Yamaji, "Part 5.5 Performance and Degradations, Chapter Impact of impurities on Materials Reliability in SOFC Stack/Modules," to be published in "Handbook of Fuel Cells Fundamentals Technology and Application, Vols. 5 and 6. Advances in Electrocatalyst, Materials, Diagnotics, and Durability, ed. W. Vielstich, H. A. Gasteiger and H. Yokokawa, John Wiley & Sons, (2009).

14. J. P. Trembly, R. S. Gemmen, D. J. Bayless, *J. Power Sources,* 163(2007) 986.

15. J. P. Trembly, R. S. Gemmen, D. J. Bayless, *J. Power Sources,* 171 (2007) 818.

16. M. Zhi, X. Chen, H. Finklea, I. Celik, and N. Q. Wu, *J. Power Sources,* 183(2008) 485.